Regulation of Human Adipose Tissue Activation, Gallbladder Size, and Bile Acid Metabolism by a β3-Adrenergic Receptor Agonist

Alison S. Baskin,[1] Joyce D. Linderman,[1] Robert J. Brychta,[1] Suzanne McGehee,[1] Esti Anflick-Chames,[1] Cheryl Cero,[1] James W. Johnson,[1] Alana E. O'Mara,[1] Laura A. Fletcher,[1] Brooks P. Leitner,[1] Courtney J. Duckworth,[1] Shan Huang,[1] Hongyi Cai,[2] H. Martin Garraffo,[2] Corina M. Millo,[3] William Dieckmann,[3] Vladimir Tolstikov,[4] Emily Y. Chen,[4] Fei Gao,[4] Niven R. Narain,[4] Michael A. Kiebish,[4] Peter J. Walter,[2] Peter Herscovitch,[3] Kong Y. Chen,[1] and Aaron M. Cypess[1]

Diabetes 2018;67:2113–2125 | https://doi.org/10.2337/db18-0462

β3-adrenergic receptor (AR) agonists are approved to treat only overactive bladder. However, rodent studies suggest that these drugs could have other beneficial effects on human metabolism. We performed tissue receptor profiling and showed that the human β3-AR mRNA is also highly expressed in gallbladder and brown adipose tissue (BAT). We next studied the clinical implications of this distribution in 12 healthy men given one-time randomized doses of placebo, the approved dose of 50 mg, and 200 mg of the β3-AR agonist mirabegron. There was a more-than-dose-proportional increase in BAT metabolic activity as measured by [^{18}F]-2-fluoro-D-2-deoxy-D-glucose positron emission tomography/computed tomography (medians 0.0 vs. 18.2 vs. 305.6 mL · mean standardized uptake value [SUV_{mean}] · g/mL). Only the 200-mg dose elevated both nonesterified fatty acids (68%) and resting energy expenditure (5.8%). Previously undescribed increases in gallbladder size (35%) and reductions in conjugated bile acids were also discovered. Therefore, besides urinary bladder relaxation, the human β3-AR contributes to white adipose tissue lipolysis, BAT thermogenesis, gallbladder relaxation, and bile acid metabolism. This physiology should be considered in the development of more selective β3-AR agonists to treat obesity-related complications.

The imbalance between energy intake and expenditure has caused escalating rates of obesity and metabolic disease throughout the world. In response to this public health crisis, the National Institutes of Health (NIH) called for the development of novel approaches for the prevention and treatment of these conditions. One focus has been on activating the β3-adrenergic receptor (AR), which in rodent models increases energy expenditure and improves glucose tolerance (1). These effects are thought to come primarily through the activation of β3-ARs expressed by brown adipose tissue (BAT), since it consumes glucose and lipids at high rates to generate heat via mitochondrial uncoupling protein 1 (UCP1) (2–4). Rodent studies have shown that an increase in BAT metabolic activity also improves insulin sensitivity, triglyceride clearance, and hepatic fatty acid oxidation (5–8). In addition, recent reports have identified multiple potential roles for BAT as an endocrine organ (8–11), often through activation of the β3-ARs.

Unfortunately, translation of these promising findings to humans has not yet been successful. Several pharmaceutical companies developed β3-AR agonists for the treatment of obesity, but none progressed past phase 2 clinical trials. Limiting factors included varied oral bioavailability (12), but ultimately the drugs did not sufficiently

[1]Diabetes, Endocrinology, and Obesity Branch, Intramural Research Program, National Institute of Diabetes and Digestive and Kidney Diseases, National Institutes of Health, Bethesda, MD
[2]Clinical Mass Spectrometry Core, National Institute of Diabetes and Digestive and Kidney Diseases, National Institutes of Health, Bethesda, MD
[3]Department of Positron Emission Tomography, National Institutes of Health, Bethesda, MD
[4]BERG, Framingham, MA

Corresponding author: Aaron M. Cypess, aaron.cypess@nih.gov.

Received 23 April 2018 and accepted 21 June 2018.

Clinical trial reg. no. NCT01950520, clinicaltrials.gov.

This article contains Supplementary Data online at http://diabetes.diabetesjournals.org/lookup/suppl/doi:10.2337/db18-0462/-/DC1.

K.Y.C. and A.M.C. contributed equally to this work.

increase energy expenditure. Nevertheless, there were beneficial outcomes, including improved glucose tolerance (13) and increased fatty acid oxidation (14), suggesting that this class of drugs could be repurposed for treating metabolic disease. These observations also suggested that there were undefined, fundamental differences between rodent and human receptor physiology that needed to be addressed so that the therapeutic promise of β3-AR agonists could be achieved.

This potential changed dramatically with the recent approval of the β3-AR agonist mirabegron (Myrbetriq, extended-release tablet; Astellas Pharma) for the treatment of overactive bladder (OAB). Though not the target tissue of interest for treatment of metabolic disease, the availability of mirabegron enabled us to determine its effects on human BAT through a pilot study where we demonstrated that it acutely stimulates BAT activity and increases resting energy expenditure (REE) in healthy subjects (15). While encouraging, that study evaluated only the 200-mg dose, which exceeds the 50-mg maximum dosage approved to treat OAB. These initial results led to the primary end point of the current study, which is whether 50 mg mirabegron, the dose shown to be safe in humans, could also acutely activate BAT and increase REE. However, we also wanted to address more fundamental physiological questions related to human β3-AR physiology and determine the breadth of the metabolic effects this new class of approved drugs can produce. We utilize tissue mRNA expression in mice and humans, pharmacokinetics, and plasma metabolomics to obtain data that could guide the development of β3-AR agonists to treat an expanded platform of obesity-related metabolic complications.

RESEARCH DESIGN AND METHODS

Study Approval

This clinical trial was registered with ClinicalTrials.gov (NCT01950520) and has U.S. Food and Drug Administration (FDA) Investigational New Drug registration no. 116246. It was approved by the Human Studies Institutional Review Board of the National Institute of Diabetes and Digestive and Kidney Diseases (NIDDK). Healthy volunteers were recruited by word of mouth or through the Patient Recruitment and Public Liaison Office and provided written informed consent.

Subject Information and Protocol Design

Inclusion criteria were as follows: generally good health, men between ages 18 and 35 years, and written informed consent. Exclusion criteria have been described previously (16). This study was randomized and placebo controlled. Only men were recruited because the 200-mg dose has been shown to cause too long of a QT prolongation in women (17). The study comprised a screening and up to four study visits, each separated by ≥48 h and completed within an 8-week window to limit outdoor temperature variation (18) and subject weight change. Subjects were asked to keep consistent weight-maintenance diets and exercise habits over the course of the study. Body composition and anthropometric measurements were taken on the first or second study day.

Healthy volunteers were admitted to the Metabolic Clinical Research Unit (MCRU) at the NIH Hatfield Clinical Research Center the evening before testing. Volunteers were provided an isocaloric dinner (55% carbohydrate, 15% protein, and 30% fat) and snack (high carbohydrate and high protein) that evening. Subjects fasted from 0000 h until completing all testing the following day. Inpatient rooms were kept at 24°C, and subjects were asked to go to sleep at the same time each night. Clothing was standardized during each metabolic chamber stay as previously described (19).

All study visits involved a 6-h (0800–1400 h) stay in the metabolic chamber of the MCRU. The relative humidity of each chamber was controlled between 30 and 50%. To reduce the likelihood of a false negative drug effect on BAT activation, on the first study day we treated subjects with cold to confirm the presence of detectable BAT. On the cold day, the chamber was set to 20°C and subjects wore a cooling vest (CFA-9 vest; Polar Products, Stow, OH) that circulated water at 14–16°C from 1200 to 1400 h. On drug study days, the chamber's temperature was set to 26°C to ensure that BAT was not activated by cold. Study subjects were administered mirabegron at 0900 h (0 min). Five hours after entering the chamber (1300 h), volunteers were injected with a 185-MBq (5 mCi) bolus of [^{18}F]-2-fluoro-D-2-deoxy-D-glucose (^{18}F-FDG) for positron emission tomography (PET)/computed tomography (CT) scanning, after which subjects spent an additional 60 min inside the chamber to allow for uptake of the radioactive tracer. PET/CT images were acquired and analyzed as previously described (20). If BAT was detected after cold exposure, the subject proceeded to the full course of drug treatment (placebo or 50 or 200 mg mirabegron). If BAT was not detected, the subject only received one drug treatment (200 mg mirabegron). Self-reported questionnaires taken at 0830 h, 1015 h, 1200 h, and 1345 h show that the subjects felt increasingly cold starting 30–60 min after entering the metabolic chamber on the cold exposure day but not on the drug treatment days.

While in the chamber, subjects were asked to minimize their physical activity and stay awake. Between 0825–0855 h and 1310–1340 h, volunteers sat upright and still without any physical activity. These inactive periods provided motion-free data to calculate REE and heart rate. Pre- and posttreatment blood samples used to measure blood metabolites were obtained 5 min prior to entering the metabolic chamber and at 1300 h. Blood samples, tested for plasma glucose, serum insulin, and plasma mirabegron concentrations, were obtained at 0, 15, 30, 60, 120, 180, 240, 315, 360, and 420 min relative to the time of drug administration (0900 h). We report only the first 8 of 10 measurements for glucose and insulin, since subjects ended their fasting after 315 min and were mobile outside of controlled conditions.

Eleven of 13 enrolled subjects completed all four study days. One subject was unable to complete the placebo study day owing to scheduling constraints. Another subject did not have detectable BAT with cold exposure and thus

completed only the 200-mg drug day. Data from this subject were included only in omics analyses. Of note, one subject completed the study within 12 weeks rather than the described 8-week period. There was no evidence of physiological changes including body weight in this subject over the more extended period.

Quantification of Tissue Metabolic Activity

BAT was quantified as previously described (20). Gallbladder volume was quantified using reconstructed PET/CT scans uploaded into Fiji (ImageJ 1.51k). A reviewer who was blinded to treatment used the CT scans to draw regions of interest that were traced around the gallbladder in each axial slice (20–40 slices per subject). If the gallbladder was indistinguishable from the nearby tissue of the liver by CT density alone, the reviewer used a coregistered PET/CT image as a guide because the liver has a higher ^{18}F-FDG uptake compared with gallbladder. A representative sample of 10 scans was reanalyzed by the same reviewer to compare volume measurements with those from the initial analysis. A paired *t* test between these values demonstrated consistency in measurement ($P = 0.94$; mean difference 5.8%). A Bland-Altman plot showed no mean or magnitude biases.

Gene Expression in Adult Humans and Mice

Tissue from 12 autopsies (5 women and 7 men aged 16–84 years) conducted at the NIH Clinical Center was collected from the following anatomic sites: superficial subcutaneous fat from the anterior abdomen, deep visceral fat from the omentum, deep supraclavicular fat, intercostal skeletal muscle, left heart ventricle, gallbladder, and urinary bladder. Resected tissue was rinsed in PBS and placed immediately in RNAlater (Qiagen). From four C57BL/6 mice maintained at 22°C, we dissected the following tissues: inguinal white adipose tissue (iWAT), epididymal WAT, interscapular BAT, tibialis anterior skeletal muscle, left and right ventricle, gallbladder, and urinary bladder. These tissues were harvested after sacrifice and were snap frozen. RNA was extracted by homogenizing 100 mg tissue using an RNeasy Mini Kit (Qiagen) according to the manufacturer's instructions. Total RNA concentration and purity were determined by spectrophotometer at 260 nm (NanoDrop 2000 UV-Vis Spectrophotometer; Thermo Scientific). RNA (1 μg) was converted to cDNA using the High-Capacity cDNA Reverse Transcription Kit (Applied Biosystems). Relative quantification of mRNA was performed with 3.5 μL cDNA used in an 11.5-μL PCR reaction for *Actb* (β-actin), *Adrb3* (β3-AR), and *Ucp1* using SYBR (Bio Basic) for mouse genes and TaqMan Gene Expression Assay for human genes (Supplementary Table 1). Quantitative RT-PCR assays were run in duplicates and quantified in the ABI Prism 7900 sequence-detection system. All genes were normalized to the expression of the housekeeping gene β-actin. For the human tissue, expression was normalized to the subcutaneous fat; in the mice, expression was normalized to the iWAT depot. Results are expressed as ratios in arbitrary units. For the comparison of adipose tissues obtained from mice raised at 22°C and thermoneutrality (30°C), six mice were raised and handled as previously described (21).

Physiological and Clinical Measurements

The NIH MCRU metabolic chamber was used to assess REE as previously described (20). A portable electrocardiogram Holter monitor (Spacelabs Healthcare), worn by the subjects, continuously measured heart rate during the time in the metabolic chamber. Subjects used the DINAMAP Pro 300 V2 monitor (GE Healthcare, Madison, WI) to take their blood pressure every 15 min. To obtain a single pre- and posttreatment blood pressure measurement for each subject, we averaged three measurements from before (0815, 0825, and 0855 h) and after (1300, 1310, and 1340 h) cold or drug administration. DXA whole-body scanner (iDXA; GE Healthcare) provided subject body composition. Subjects answered two questionnaires via iPad, version 2 (Apple, Cupertino, CA), during their metabolic chamber stays. One assessed whether they were experiencing any responses to treatment, and the second comprised a visual analog scale to assess overall comfort, including temperature perception, hunger, and energy.

Measurement of Plasma Mirabegron and 7α-Hydroxy-4-Cholesten-3-One Concentrations via Ultraperformance Liquid Chromatography–Tandem Mass Spectrometry Analysis

Detection and quantification were achieved by ultraperformance liquid chromatography–tandem mass spectrometry utilizing a Thermo Scientific Vanquish ultra-high-performance liquid chromatography. For mirabegron, we used a Thermo Scientific Quantiva or Altis triple quadrupole mass spectrometer with heated electrospray ionization (HESI-II; Thermo Scientific) in positive ion mode (3,500 V). Quantitation of mirabegron was based on the mass/charge transitions 397→146 and 397→260 and internal standard ($^{13}C_6$-mirabegron) 403→152 and 403→266. Quantitation of 7α-hydroxy-4-cholesten-3-one (C4) was based on the mass/charge transitions 401→177 and 401→383 and D_7-C4 on 408→177 and 408→390 transitions. For mirabegron, the calibration stock solutions (1–250 ng/mL) and internal standard solution were prepared in acetonitrile and stored at 4°C. Calibration and plasma samples were prepared by protein precipitation with internal standard solution, vortexed, kept at 4°C for 10 min, and then centrifuged at 4°C, 14,000 rpm, for 15 min. The supernatant was transferred to liquid chromatography–mass spectrometry (LC-MS) vial with 1 μL injected. A Waters Acquity UPLC BEH C18, 2.1 × 100 mm, 2.7-μm column was maintained at 35°C. Solvent A comprised 70% H_2O and 30% acetonitrile with 0.1% NH_3 and solvent B 20% H_2O and 80% acetonitrile with 0.1% NH_3. The flow rate was 400 μL/min and the gradient was 25% B at 0 min increasing to 100% B at 4.5, maintaining 100% B until 5 min, returning to 25% B at 5.5 min.

For plasma C4 concentrations, the internal standard solution was prepared in methanol containing D_7-C4. C4 standard stock solutions were prepared in methanol at the

concentrations from 0.5 to 100 ng/mL. All standard stock solutions were stored at 4°C. Calibration and plasma samples were prepared by protein precipitation with internal standard solution, vortexed, kept at 4°C for 10 min, and then centrifuged at 4°C, 14,000 rpm, for 15 min. The supernatant was transferred to an LC-MS vial with 3 μL injected. A Waters Acquity UPLC BEH C18, 2.1 × 100 mm, 2.7-μm column was maintained at 35°C. Solvent A comprised H_2O with 5 mmol/L NH_4OAc, and solvent B methanol with 5 mmol/L NH_4OAc. The flow rate was 300 μL/min and the gradient was 35% B at 0 min, increasing to 98% B at 3.5 min, remaining at 98% B until 6.9 min, and returning to 35% B at 7.25 min. Calibration standards of mirabegron and C4 were used to construct calibration curves, which had a minimum $R^2 \geq 0.999$ with $1/x$ weighting. Calibration and repeat measurement of standards exceeded FDA LC-MS guidelines for linearity and quantitation.

Measurement of Metabolites

Glucose, insulin, nonesterified fatty acids (NEFAs), total triiodothyronine, free thyroxine, thyrotropin, lactate, cortisol, norepinephrine, epinephrine, and dopamine were all measured by the NIH Department of Laboratory Medicine. For epinephrine and dopamine concentrations that were below the assay detection limit, we imputed the half-minimum value. Pyruvate was measured by the Mayo Clinic (Mayo Clinic Laboratories). β-Hydroxybutyrate (BHB), glycerol, and metabolic proteins and hormones were measured at the NIDDK Clinical Core Lab. Colorimetric assay kits were used to measure BHB and glycerol (Cayman Chemical) and total bile acids (Diazyme Laboratories). FGF19, FGF21, and adiponectin were measured using Quantikine ELISA kits (R&D Systems). Ghrelin (active), PYY, leptin, and GIP were measured using the Human Metabolic Hormone Magnetic Bead Panel Metabolism Multiplex Assay (EMD Millipore). Glucagon was measured using an ELISA kit (Mercodia). Active glucagon-like peptide 1 was measured using the Active GLP-1 (version 2) Kit (Meso Scale Discovery).

Metabolomics

Metabolomic analyses were performed using nontargeted and targeted protocols as previously described (22–24). Plasma samples were collected in K2-EDTA tubes before and after treatment with cold exposure or mirabegron. Metabolite extraction was achieved using a mixture of isopropanol:acetonitrile:water (3:3:2 v/v). Extract analysis were performed using gas chromatography–mass spectrometry, reversed-phase LC-MS, and hydrophilic interaction chromatography–liquid chromatography–tandem mass spectrometry protocols as previously described (24). A quality control was performed using metabolite standards mixture and pooled samples. Collected raw data were manually inspected, merged, and imputed. Statistical analysis was performed with MetaboAnalyst 3.0 (25). Metabolite Set Enrichment Analysis (MSEA) was used to interrogate functional relation, which describes the correlation between compound concentration profiles and clinical outcomes.

For the determination of the relationships between plasma bile acid levels and mirabegron dose, we performed a data integrity check, missing value imputations, data filtering, and normalization by the sample median. We first determined whether there was a relationship between mirabegron dose and bile acid levels using means comparison with dose treated as a continuous variable, which identified four bile acids with $P < 0.05$. This test was followed by one-way means comparisons between the average baseline levels of the bile acids combining the placebo, 50-mg, and 200-mg days (n = 36), and the post-treatment levels of the three different treatment days, each assessed individually (n = 11–13). P values for all pairs were calculated using the Tukey-Kramer honest significant difference test.

Sample Size Calculation

Our previous study showed that $\log_{10}$ BAT activity was normally distributed, with values of 0.05 ± 0.62 mL · mean standardized uptake value (SUV_{mean}) · g/mL at a dose of placebo and 2.00 ± 0.79 mL · SUV_{mean} · g/mL at a dose of 200 mg mirabegron (15). Because the current study was the first to explore the effect of 50 mg mirabegron on BAT activity, a range for activation of BAT with 50 mg mirabegron was calculated based on lower- and upper-bound expectations about the reported pharmacokinetic/pharmacodynamic profile. We predicted that the 50-mg dose would produce a mean $\log_{10}$ BAT activity of 0.36 mL · SUV_{mean} · g/mL with an SD of 0.66, assuming a linear relationship between dose and SD. BAT activity was treated as a continuous variable, and each subject served as his own paired control. We determined that 12 subjects would be needed to reject the null hypothesis that the response difference between placebo and 50 mg mirabegron is 0 in a paired comparison with α = 0.05 and power 80%.

Statistical Methods

After completion of the study in 12 subjects with detectable BAT, data were analyzed with JMP 11.0.0 software (SAS Institute, Inc.) and GraphPad Prism 7.0 (GraphPad Software, Inc.). To evaluate the primary end point, we used a paired t test on log-transformed data and found that P = 0.003 after imputing for measurements of "0" the values that were one-half of the detectable lower limit of the imaging software. All other paired comparisons were performed using either Student paired t tests or Wilcoxon signed rank tests depending on the current or historical distribution of underlying data. We used repeated-measures ANOVA to determine whether pretreatment values measured on the placebo, 50-mg, and 200-mg study days were significantly different from each other. Associations between study variables were determined using random effects linear regressions. Before analyzing the data, we confirmed that there was no significant effect of a possible interaction between the assigned drug dose and its study visit number

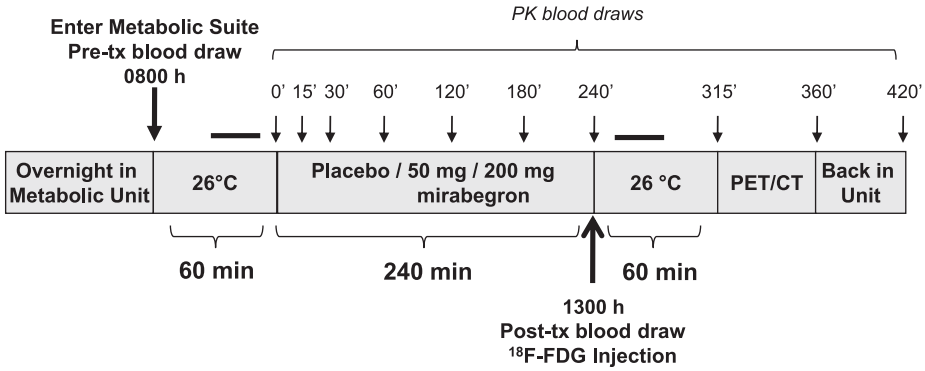

Figure 1—Study design. Subjects entered the metabolic chamber at 0800 h and remained there until 1400 h, after which they were transported to the PET/CT suite. Blood was drawn before treatment (tx) at 0800 h and then just prior to ^{18}F-FDG administration at 1300 h. The black bars above the diagrams refer to the 30-min still periods during which REE was measured. PK, pharmacokinetic.

on other variables; furthermore, drug dose and study visit were not predictive of each other. All *P* values are two tailed, with statistical significance being *P* values $\leq$0.05.

RESULTS

Dose-Dependent BAT Activation by Mirabegron

In the current study (Fig. 1), we enrolled 13 young, lean, and healthy men, 12 of whom (Table 1) had detectable cold-activated BAT (Supplementary Fig. 1). Compared with placebo, 50 mg mirabegron increased BAT activity in most subjects (medians 0.0 vs. 18.2 mL · SUV_{mean} · g/mL, *P* = 0.008) (Supplementary Fig. 1). However, BAT activation with 50 mg was significantly less than with 200 mg (median 305.6 mL · SUV_{mean} · g/mL, *P* = 0.007) (Fig. 2*A* and *B* and Supplementary Fig. 1).

Table 1—Demographics of study subjects*

	Value	Range
Sex (*n* men/women)	12/0	—
Age (years)	24.7 ± 4.0	(19.1–31.7)
Height (cm)	183.2 ± 5.3	(174.9–194.4)
Weight (kg)	78.9 ± 8.9	(66.5–93.9)
BMI (kg/m^2)	23.5 ± 1.9	(20.3–26.1)
Body surface area (m^2)‡	2.0 ± 0.1	(1.8–2.2)
Body fat (kg)	12.8 ± 4.6	(6.3–22.1)
Total percent fat (%)	16.3 ± 5.1	(7.7–24.6)
Total fat-free mass (kg)	65.5 ± 7.9	(54.3–77.9)
Total lean mass (kg)	62.1 ± 7.5	(51.6–73.6)
Total percent lean mass (%)	79.3 ± 5.0	(71.1–88.1)
Total bone mineral content (kg)	3.4 ± 0.5	(2.7–4.3)
Resting HR (bpm)§	65 ± 8	(46–76)
Resting SBP (mmHg)§	120 ± 6	(108–131)
Resting DBP (mmHg)§	70 ± 6	(62–81)
Resting RPP (mmHg · bpm)§	7,780 ± 1,011	(5,823–9,957)
REE (kcal/h)§	77.4 ± 10.0	(63.5–96.0)

Data are means ± SD unless otherwise indicated. DBP, diastolic blood pressure; HR, heart rate; RPP, rate pressure product; SBP, systolic blood pressure. *Measured at screening. §Value = the average of the pretreatment values measured on the days when mirabegron or placebo were given. ‡Calculated as previously described (60).

Varied Tissue Distribution of the β3-AR and UCP1

The greater BAT activation with 200 mg compared with 50 mg mirabegron is different from its effects on OAB, where the two doses are equally effective (26). On the other hand, β3-AR agonists potently activate BAT thermogenesis in mice, without much effect on bladder relaxation (27,28). To address these apparent tissue and species differences, we measured β3-AR and UCP1 mRNA levels in multiple organs in mice and a separate group of humans. In mice, both the β3-AR and UCP1 mRNA levels were orders of magnitude higher in both BAT and WAT than other tissues (Fig. 2*C* and *D*). For example, the ratio of β3-AR expression in inguinal WAT compared with urinary bladder was 77:1. In contrast, the human β3-AR was most highly expressed in the urinary bladder, with a subcutaneous WAT:urinary bladder 1:78, a range of three orders of magnitude (Fig. 2*E* and *F*). UCP1, while generally higher in the human supraclavicular adipose depot compared with WAT, was not as distinctly "brown" as mouse interscapular BAT (29). Of note, the data shown are from tissue that was obtained from humans who lived at thermoneutrality (22°C), though the mice raised at this temperature experienced cold stress. We compared the mRNA levels of the β3-AR in the WAT and BAT in a separate set of mice raised at 22°C and mouse thermoneutrality (30°C), and they were not different (all $P > 0.05$). Nevertheless, the difference in housing temperatures may limit the interpretation of the mouse-human comparisons.

More-Than-Dose-Proportional Pharmacokinetics

Mirabegron plasma exposure (Fig. 3*A*) increased in a more-than-dose-proportional manner as previously reported (17) (Supplementary Table 2). There was a robust positive dose-response relationship between mirabegron and BAT activity (Supplementary Tables 3 and 4). Of note,

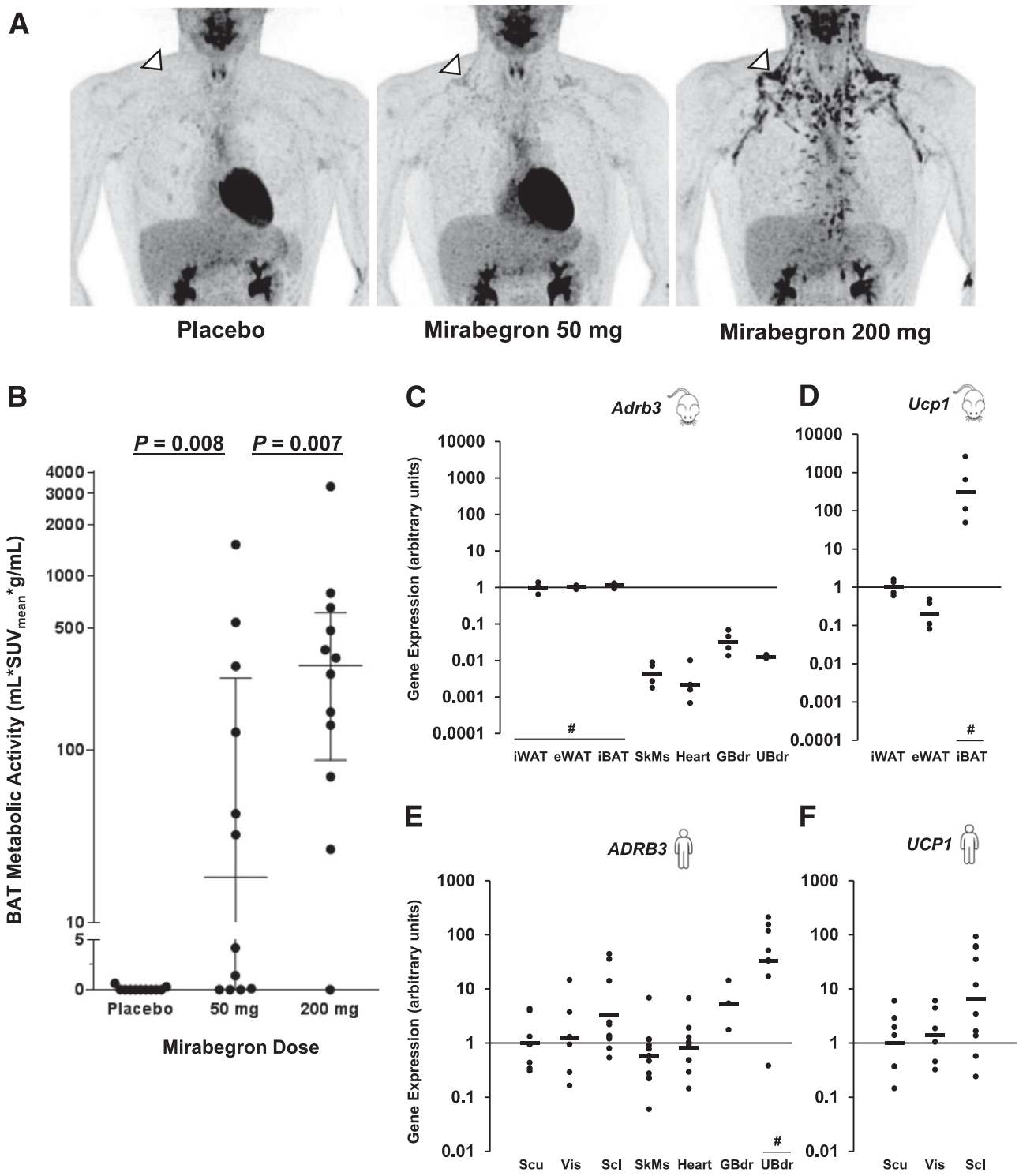

Figure 2—Mirabegron activation of BAT and tissue β3-AR expression. *A*: PET images demonstrating the dose-dependent pattern of BAT activation in a representative subject. The supraclavicular BAT depot is identified by the white arrowhead. *B*: Mirabegron-induced BAT metabolic activity in the 12 subjects who had detectable cold-activated BAT after a single dose of placebo, 50 mg mirabegron, and 200 mg mirabegron. For the 50-mg and 200-mg doses, the wider lines are the group medians and the narrower upper and lower lines show the interquartile ranges. The *P* values for the nonparametric Wilcoxon signed rank tests are shown. mRNA expression of the β3-AR (*Adrb3*) (*C*) and *Ucp1* (*D*) in mouse iWAT, epididymal WAT (eWAT), interscapular BAT (iBAT), skeletal muscle (SkMs), heart myocardium (Heart), gallbladder (GBdr), and urinary bladder (UBdr). Expression was normalized to the iWAT depot geometric mean; $n = 4$ for each of the sites. mRNA expression of the β3-AR (*ADRB3*) (*E*) and *UCP1* (*F*) in human subcutaneous WAT (Scu), visceral WAT (Vis), supraclavicular BAT (Scl), skeletal muscle, heart myocardium, gallbladder, and urinary bladder. Expression was normalized to the human subcutaneous WAT depot geometric mean. $n = 3$–12 postmortem subjects. Black bars are the geometric means. #*P* values <0.05 compared with other depots for all paired comparisons using Tukey-Kramer honest significant difference tests.

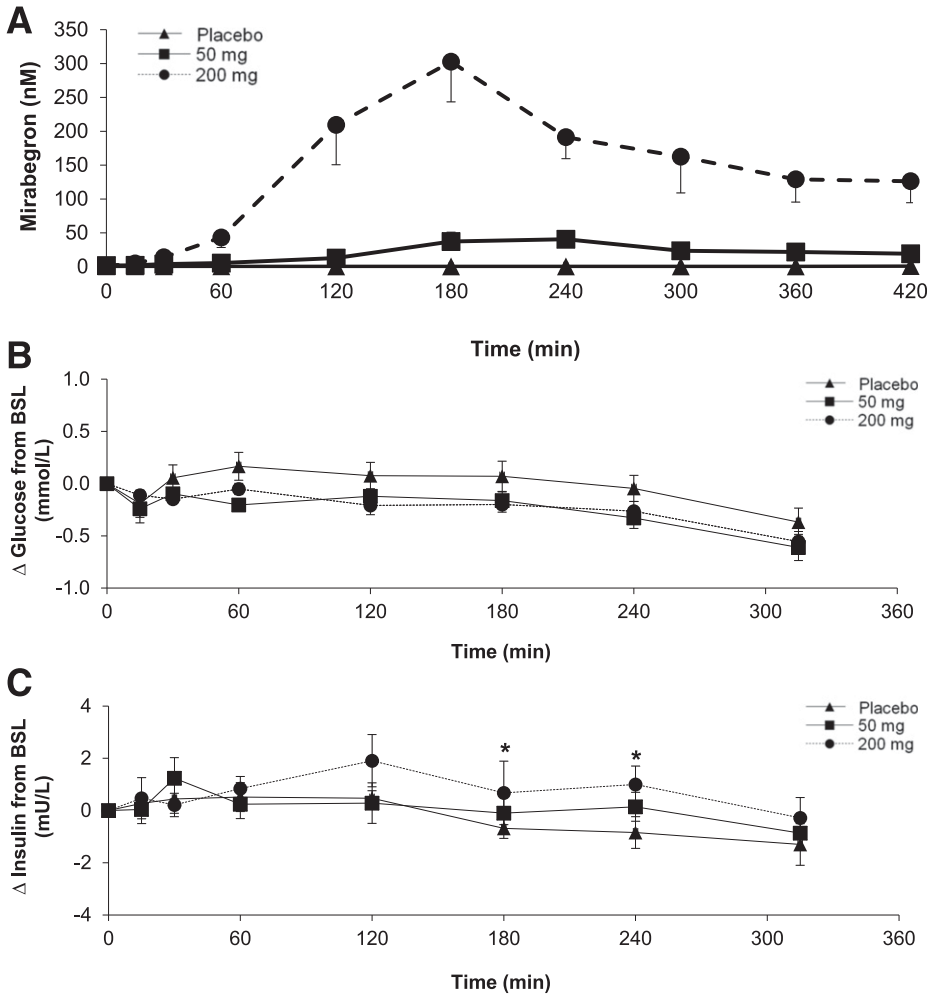

Baseline levels (t = 0 min), all $P > 0.05$			
Metabolite	Placebo	50 mg	200 mg
Glucose (mg/dL)	4.9 ± 0.2	5.1 ± 0.1	5.1 ± 0.1
Insulin (mU/L)	5.3 ± 1.0	5.3 ± 0.8	6.7 ± 1.8

Change in AUC compared to placebo, all $P > 0.05$		
Metabolite	50 mg	200 mg
Glucose (mmol*h/L)	−1.2 ± 0.6	−1.2 ± 0.8
Insulin (mU*h/L)	2.2 ± 2.7	7.4 ± 3.4

Figure 3—Mirabegron pharmacokinetic and pharmacodynamic profiles. *A*: Mean plasma concentrations of mirabegron in the 12 subjects who had detectable cold-activated BAT after taking a single dose of placebo, 50 mg mirabegron, and 200 mg mirabegron. Changes in plasma glucose (n = 11) (*B*) and insulin (n = 6) (*C*) after oral administration of placebo and 50 and 200 mg of the β3-AR agonist mirabegron. The baseline (BSL) levels are shown in the inset table on the left and the changes in area under the curve (AUC) in the inset table on the right. Values are mean ± SEM. For individual time points, * indicates paired t tests with $P < 0.05$.

the BAT response to the 50 mg dose was quite variable, including three subjects who had detectable BAT with 200 mg but not with 50 mg mirabegron. These data suggest that in contrast to the equivalent effects on the bladder with both doses, even higher exposures to mirabegron might lead to greater increases in BAT metabolic activity in many subjects.

Limited Metabolic, Hormonal, and Cardiovascular Response to Mirabegron

We assessed the effects of mirabegron on metabolites and hormones by comparing levels before and after drug administration (Supplementary Table 5). Baseline values across study days were not different for any hormone. Levels of thyrotropin, cortisol, ACTH, FGF21, leptin, and glucagon-like peptide 1 decreased during the study days for all treatments, which is consistent with diurnal rhythms and/or a physiological response to fasting (30–35). NEFAs and BHB increased with increasing doses of mirabegron, reflecting β3-AR–mediated lipolysis in WAT and subsequent hepatic ketogenesis. Total bile acids and FGF19 were decreased with all treatments. However, there was no change in C4, a plasma biomarker that reflects the activity of CYP7A1, the hepatocellular enzyme that is the rate-determining step for bile acid synthesis from cholesterol. Glucose and insulin were also measured serially, and both did not substantially change from their baselines. One pattern of potential physiological significance was that the

200-mg dose of mirabegron led to higher insulin levels compared with placebo: the change in area under the curve was 7.4 ± 3.4 mU · h/L, P = 0.07 (Fig. 3*B* and *C*). These small changes contrast with the marked hyperinsulinemia seen after β3-AR agonist treatment in rodents (36).

There were dose-dependent increases from pretreatment measurements in heart rate (5.1 ± 2.1 bpm for 200 mg, P = 0.03), systolic blood pressure (6.8 ± 2.4 mmHg for 200 mg, P = 0.02), diastolic blood pressure (1.4 ± 1.4 mmHg for 200 mg, P = 0.34), and rate pressure product, a correlate of myocardial oxygen consumption (1,095 ± 304 bpm · mmHg for 200 mg, P = 0.004) (Supplementary Fig. 2 and Supplementary Table 6) (37,38). This cardiovascular stimulation is consistent with our previous study of mirabegron (15) and demonstrates why the 200-mg dose is not used clinically. Per self-administered questionnaires, subjects did not report any treatment-emergent adverse effects for either dose.

Changes in REE Limited to 200 mg

Pretreatment REE values measured prior to placebo, 50-mg, and 200-mg days were not different (P = 0.99), and REE did not increase in response to either placebo or 50 mg (Fig. 4*A* and *B*). In contrast, the 200-mg dose increased REE by 5.8% (4.5 ± 5.5 kcal/h, P = 0.02) (Fig. 4*C*). There was a positive relationship between mirabegron dose (P = 0.01) and other pharmacokinetic parameters and the average change in REE (Supplementary Table 6). In addition to mirabegron dose, we found a significant relationship between BAT metabolic activity and the change in REE (P = 0.002) (Fig. 4*D*). Multiple linear regression showed that the change in REE was predicted by both change in rate pressure product (P = 0.003) and BAT activity (P = 0.014) (Supplementary Table 7). These data indicate that mirabegron increases energy expenditure via both cardiovascular stimulation and BAT thermogenesis.

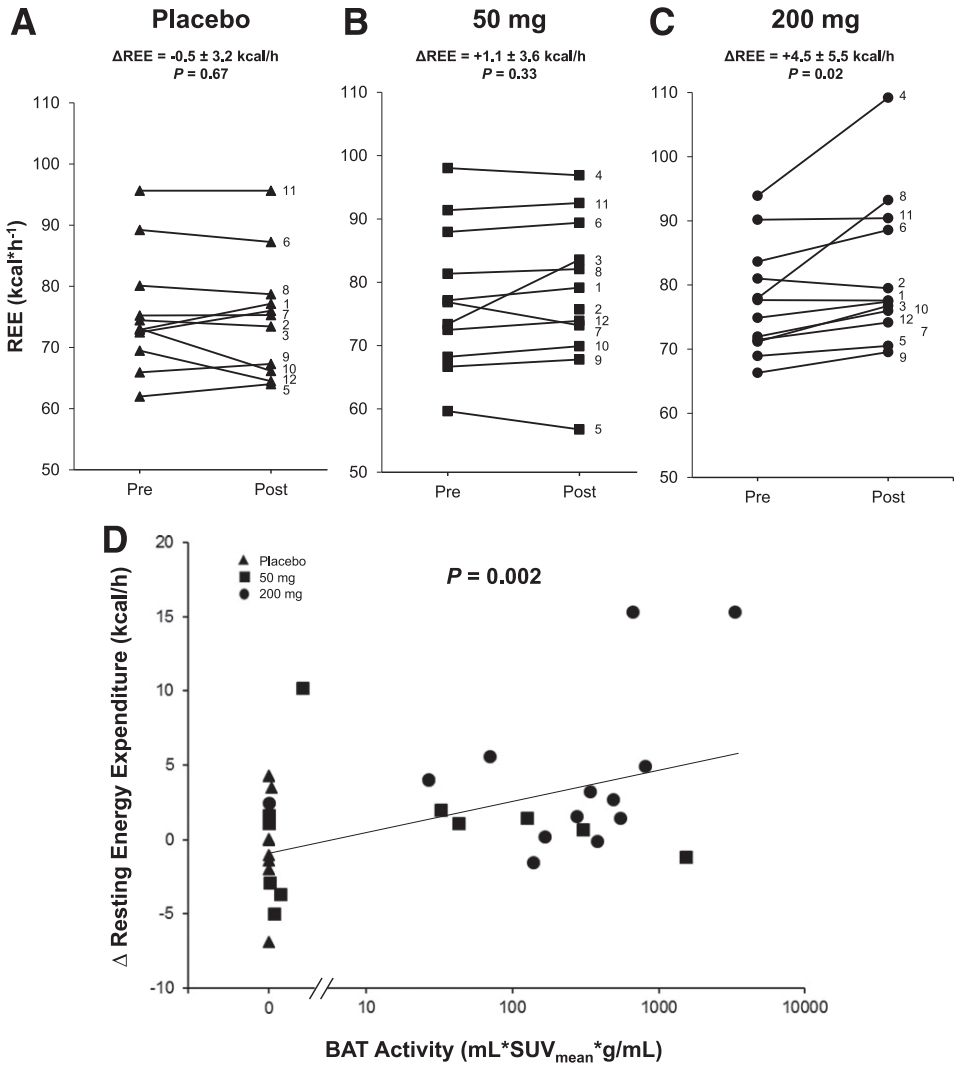

Figure 4— Effects of mirabegron and BAT activity on REE. Change in REE as measured in a metabolic chamber during 20-min still periods as described in RESEARCH DESIGN AND METHODS after dosing with placebo (triangles) (*A*), 50 mg mirabegron (squares) (*B*), and 200 mg mirabegron (circles) (*C*). P values shown are for the paired Student t tests comparing pretreatment (Pre) (0800 h) with posttreatment (Post) (1300 h, the time of ^{18}F-FDG injection). *D*: Relationship between the change in REE and BAT metabolic activity. P values were determined using a linear mixed-effects model to account for each subject taking three different doses of medication. n = 34.

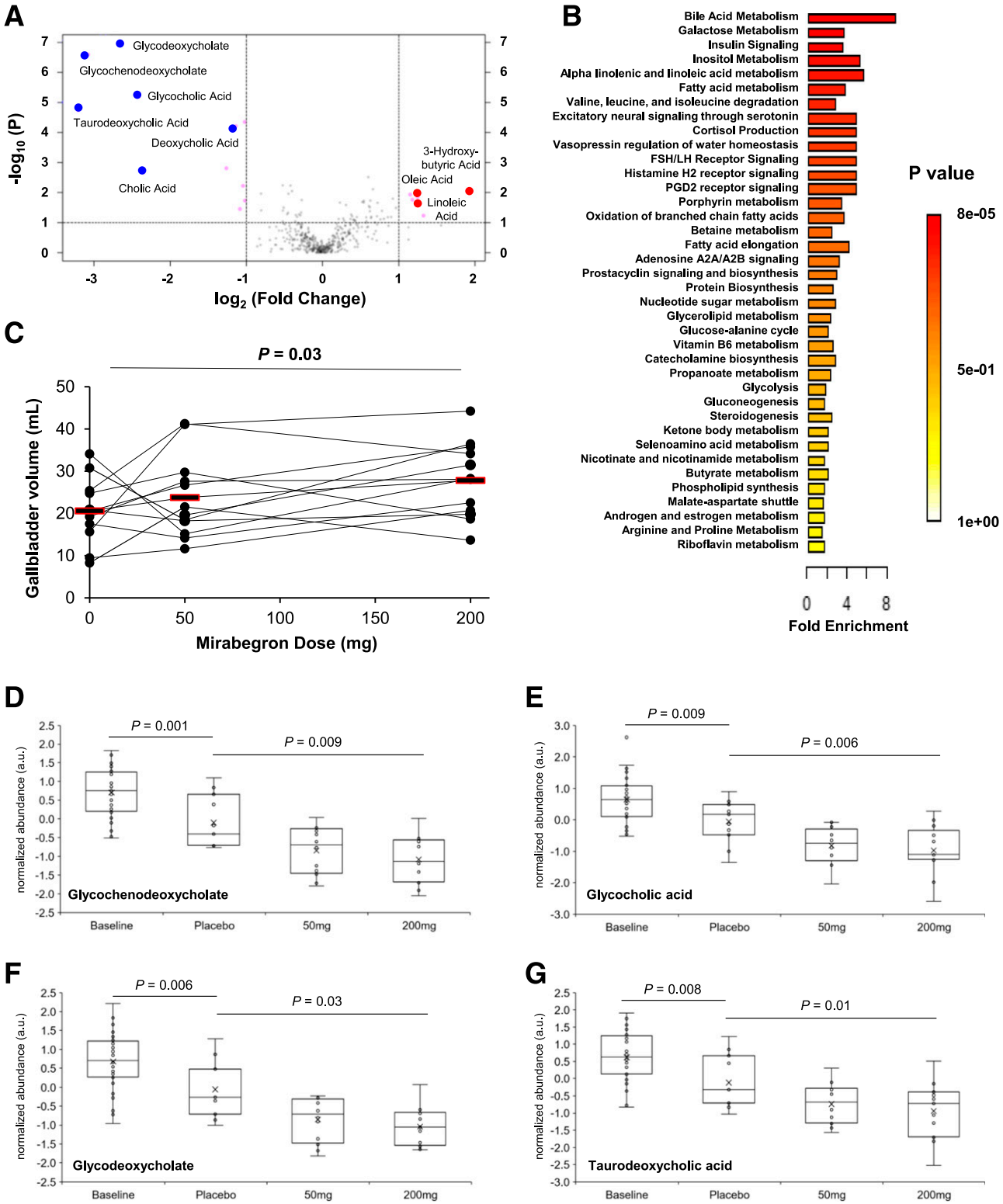

Figure 5—Metabolomic analysis after exposure to the β3-AR agonist mirabegron. *A*: Volcano plot of 443 metabolites comparing the fold induction before and then after oral administration of 200 mg mirabegron. The vertical lines indicate changes $\log_2$-fold >1.0 or <1.0. The horizontal line indicates $-\log_{10} P$ values >1.3 ($P < 0.05$) based on paired Student *t* tests. Metabolites meeting those criteria are shown by magenta circles, with bile acids (decreased, blue circles) and long-chain fatty acids (increased, red circles) named. $n = 13$. *B*: Quantitative enrichment analysis of the metabolic pathways most affected by treatment with 200 mg mirabegron. $n = 13$. *C*: Relationship between mirabegron dose and gallbladder size. Red bars are sample means. *D*–*G*: Dose-response effects of mirabegron on plasma bile acid levels. For glycochenodeoxycholate (*D*), glycocholic acid (*E*), glycodeoxycholate (*F*), and taurodeoxycholic acid (*G*), the effects of fasting are shown through unpaired Student *t* tests comparing baseline ($n = 36$) with placebo ($n = 11$). The effects of mirabegron dose are shown through one-way means comparisons between the average baseline levels of the bile acids combining the placebo, 50-mg, and 200-mg days ($n = 36$) and

Drug-Induced Changes in Gallbladder Size and Conjugated Plasma Bile Acids

We next performed a metabolomic analysis of the response to mirabegron using 443 different plasma metabolites (Supplementary Data). Since 200 mg produced the most pronounced physiological effects, we focused first on that dose. There was an increase in long-chain fatty acids and 3-hydroxybutyrate (Fig. 5*A*), which is consistent with the dose-dependent increases in total serum NEFA and ketones induced by mirabegron. A second, more prominent pattern was a reduction in bile acids (Fig. 5*A*). The changes in individual metabolites were also seen in quantitative enrichment analysis of metabolic pathways (Fig. 5*B*), which showed that bile acid metabolism was the pathway most significantly affected by 200 mg mirabegron. This effect on bile acids, combined with our human tissue profiling showing elevated β3-AR mRNA expression in gallbladder (Fig. 2*E*), led us to measure gallbladder volume. Using the PET and CT images acquired as part of BAT imaging, we found that the volumes were higher after higher doses of mirabegron: 20.6 ± 8.0, 23.8 ± 9.8, and 27.8 ± 9.0 mL, respectively, for placebo, 50 mg, and 200 mg (compared with placebo, $P = 0.37$ for 50 mg and $P = 0.04$ for 200 mg). The 35% increase in gallbladder volume was dose dependent ($P = 0.03$) (Fig. 5*C*).

The reduction in plasma bile acids had two contributors: the first was due to fasting over time, and the second was from mirabegron itself. We distinguished these two effects by looking at the changes from baseline (0800–1300 h) during the placebo days. For all six bile acids measured, there was a decrease ($P < 0.05$ for each) (Supplementary Table 8). We measured the effect of mirabegron through a bivariate fit of bile acid level by mirabegron dose and then did paired means comparisons. There were mirabegron-induced reductions in all four conjugated plasma bile acids tested: glycochenodeoxycholate, glycocholic acid, glycodeoxycholate, and taurodeoxycholic acid (Fig. 5*D*–*G* and Supplementary Table 8).

DISCUSSION

After decades of clinical trials with β3-AR agonists designed to treat obesity (13,14,39,40), there is still no β3-AR agonist approved for that indication. However, recent progress indicates that the landscape is not so bleak. Evidence for this optimism is that the more selective β3-AR agonist mirabegron has been approved for the safe treatment of OAB (41). The current study shows it is worth reconsidering the feasibility of stimulating BAT thermogenesis and WAT lipolysis—and possibly regulating bile acid metabolism as well. Our primary end point addressed a fundamental question: why is weight loss not reported in clinical trials using an FDA-approved 50-mg dose of mirabegron (42)? The results here show that in a substantial proportion of the subjects, 50 mg is not a high enough dose to consistently increase REE or BAT activation. Only the 200-mg dose is effective, but it comes with undesirable activation of the cardiovascular system, likely from off-target binding to the β1-AR (17). Mechanistically, reasons for the difference in BAT and bladder outcomes derive from the lower β3-AR mRNA expression in human adipose tissues and the lower plasma exposure with 50 mg mirabegron.

Even with a more selective β3-AR agonist, the activation of human BAT thermogenesis for inducing long-term weight loss may not be successful given that increasing energy expenditure could induce compensatory increases in energy intake. However, it is not clear whether this compensation will be complete and might be significantly less. In addition, even with no weight reduction, successful chronic activation of human BAT could affect general metabolism in a positive way. Rodent studies show that chronic stimulation of BAT leads to improved glucose homeostasis and insulin sensitivity (7) and that BAT can act as an endocrine organ to regulate whole-body metabolism (6,8,10,11,43). Given the substantial similarities between rodent and human brown adipocytes at the level of cellular physiology (44,45), it is reasonable to think that β3-AR agonist-mediated activation of human BAT could treat obesity-related pathophysiology.

Beyond the expected effects on adipose tissues, mirabegron also impacts the hepatobiliary axis. The increase in gallbladder size is consistent with β3-AR binding and likely derives from cAMP-mediated relaxation of its smooth muscle (46). The reduction in plasma conjugated bile acids has not been reported previously in either rodents or humans. The mechanism does not appear to involve a change in hepatic bile acid synthesis, as there was no difference in plasma C4. Although the reduction in FGF19 levels indicates lower delivery of bile acids to the ileum, the decline appeared to be a result of fasting, as we did not identify a dose-dependent mirabegron effect. Rather, the mechanism could be through the β3-ARs expressed by hepatic stellate cells (47). When stimulated by a β3-AR agonist, these cells increase intrahepatic blood flow and could lead to a higher rate of conjugated bile acid uptake by the liver and deposition into a larger gallbladder. Consistent with this model, the plasma bile acids that declined dose dependently were conjugated species that undergo ileal transport from the small intestine into the portal circulation (Fig. 6). In contrast, deoxycholic acid, which did not change as consistently, is generated in and absorbed from the colon and reaches the liver at more variable rates (48). Alternative mechanisms may include altered bile acid transport (49), increased fecal excretion (50), and increased hepatic clearance with reduced production regulated by farnesoid X receptor

the posttreatment levels of the three different treatment days, shown individually. $n = 11–13$. In the box plots, the middle lines are the group medians and the upper and lower lines show the interquartile ranges. a.u., arbitrary units; FSH/LH, follicle-stimulating hormone/leutinizing hormone; PGD2, prostaglandin D_2.

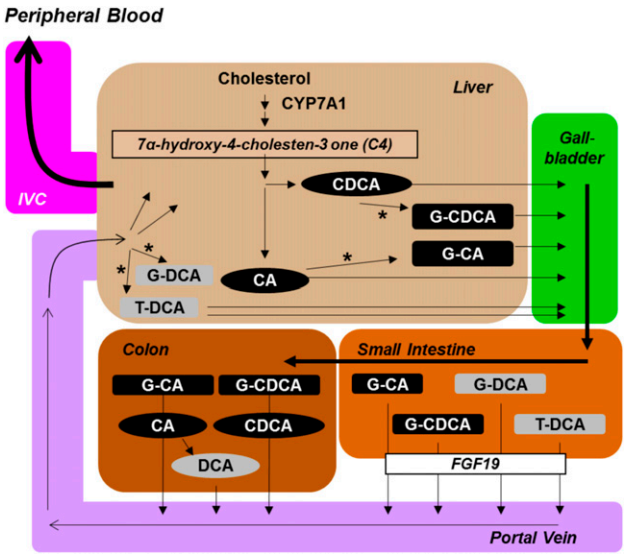

Figure 6—Bile acid processing in humans and the potential role of β3-AR agonists. For bile acid synthesis and enterohepatic cycling in humans, the hepatic enzyme that is the rate-determining step for production from cholesterol is CYP7A1. Its cellular activity is reflected by plasma C4. Primary unconjugated (black ovals) cholic acid (CA) and chenodeoxycholic acid (CDCA); primary conjugated (black rectangles) glycochenodeoxycholate (G-CDCA) and glycocholate (G-CA); secondary unconjugated (gray oval) deoxycholic acid (DCA); and secondary conjugated (gray rectangles) glycodeoxycholate (G-DCA) and taurodeoxycholate (T-DCA). The rate of ileal transepithelial bile salt flux is reflected by plasma levels of FGF19. Bile acids return to the liver; those that are not taken up are detected in the peripheral circulation, which the bile acids enter via the inferior vena cava (IVC). Closed arrowheads indicate the movement of bile acids, and open arrowheads indicate flow of blood. The * indicates a conjugation step, the addition of either choline or taurine by liver hepatocytes.

(FXR) (51,52). More studies are needed, such as calculating gallbladder volume before and after treatment and directly measuring enterohepatic bile acids at different sites, to refine the kinetics and mechanisms underlying these processes.

The ability of the β3-AR agonist mirabegron to affect the hepatobiliary axis may have clinical implications. Gallbladder relaxation may be useful in the management of cholelithiasis (53). Bile acids also have endocrine roles via the TGR5 and FXR that have multiple effects, including increasing energy expenditure and beneficially modifying the gut microbiome (54–56). These novel discoveries must be considered in the context of the limitations of this study: it comprised a small group of young, lean, healthy men with detectable BAT, so future studies need to determine the magnitude by which a β3-AR agonist activates BAT and regulates bile acid levels in women, older adults, obese subjects, and patients with other metabolic stresses.

In summary, we demonstrate that the β3-AR agonist mirabegron causes multiple dose-dependent effects in humans: increases in WAT lipolysis, BAT metabolic activity, REE, and gallbladder volume and a reduction in plasma conjugated bile acids. All of these effects were far more pronounced at the 200-mg dose, which is higher than what is approved to treat OAB. For this reason, it is likely that many of the physiological responses to β3-AR agonists in humans have not yet been reported. These findings support the development of more selective human β3-AR agonists, since activation of BAT has other beneficial effects, including protection from atherosclerosis (57), reduction in fatty liver (58), and improved glucose tolerance (7) and bile acids are emerging as pleiotropic modulators of metabolism (59). The potential for activation of the β3-AR to improve metabolic health highlights the need to further probe its physiological impacts with the goal of developing novel treatments for obesity-related metabolic disease.

Acknowledgments. The authors thank the NIDDK Clinical Research Center nursing team, NIH Clinical Center Nutrition Department, NIDDK Clinical Laboratory Core, NIH Department of Laboratory Medicine, research pharmacy, and PET technologists for the excellent support provided. The authors also thank their collaborators at BERG for technical assistance in the metabolomics work: Justice McDaniel, Brian Williams, Bennett Greenwood, and Cindy Nguyen. The authors thank David Kleiner, Mohammed Mahbood, Sarah Young, Willie Young, and the Laboratory of Pathology at the NIH Clinical Center. The authors thank Theo Heller and Rabab Ali of the NIDDK's Translational Hepatology Section for guidance in developing the assay for gallbladder volume. The authors thank Cuiying Xiao and Marc Reitman of the NIDDK for the gift of adipose tissue from mice raised at 22°C and 30°C. The authors thank Frank Gonzalez and Cen Xie of the National Cancer Institute for their perspective on bile acid metabolism. The authors are grateful to Norman Javitt of NYU Langone Medical Center for his insights regarding bile acid metabolism, enterohepatic circulation, and intrahepatic vasculature. The authors are also grateful to Sungyoung Auh of the NIDDK for biostatistical advice; Marc Reitman of the NIDDK, Jack Yanovski of the *Eunice Kennedy Shriver* National Institute of Child Health and Human Development, and Clifton Bogardus of the NIDDK for discussions about the data and their implications; and Raymond H. Cypess of the American Type Culture Collection for advice on manuscript preparation. The authors are especially thankful for the volunteers' commitment to the study.

Funding. This work was supported by the Intramural Research Program of the NIDDK: DK-075112 (to A.M.C.), DK-075116 (to A.M.C.), DK-071013 (to K.Y.C.), and DK-071014 (to K.Y.C.).

Duality of Interest. V.T., E.Y.C., F.G., N.R.N., and M.A.K. are employees of BERG. No other potential conflicts of interest relevant to this article were reported.

Author Contributions. A.S.B., J.D.L., R.J.B., S.M., B.P.L., C.J.D., and K.Y.C. conducted the physiological measurements. A.S.B., J.D.L., R.J.B., H.C., H.M.G., V.T., M.A.K., P.J.W., P.H., K.Y.C., and A.M.C. designed the experiments. A.S.B., H.C., H.M.G., V.T., M.A.K., and A.M.C. wrote the manuscript. A.S.B. and A.M.C. calculated the biostatistics. E.A.-C., B.P.L., S.H., C.M.M., W.D., and P.H. quantified BAT metabolic activity. C.C. performed the gene expression studies in mice and humans. L.A.F. quantified gallbladder volume. H.C., H.M.G., and P.J.W. measured plasma mirabegron. V.T., E.Y.C., F.G., N.R.N., and M.A.K. performed the metabolomics. A.S.B., J.D.L., R.J.B., S.M., E.A.-C., C.C., J.W.J., A.E.O., L.A.F., B.P.L., C.J.D., S.H., H.C., H.M.G., C.M.M., W.D., V.T., E.Y.C., F.G., N.R.N., M.A.K., P.J.W., P.H., K.Y.C., and A.M.C. contributed to editing the manuscript. A.M.C. is the guarantor of this work and, as such, had full access to all the data in the study and takes responsibility for the integrity of the data and the accuracy of the data analysis.

References

1. Liu X, Pérusse F, Bukowiecki LJ. Mechanisms of the antidiabetic effects of the beta 3-adrenergic agonist CL-316243 in obese Zucker-ZDF rats. Am J Physiol 1998;274:R1212–R1219

2. van Marken Lichtenbelt WD, Vanhommerig JW, Smulders NM, et al. Cold-activated brown adipose tissue in healthy men. N Engl J Med 2009;360:1500–1508

3. Cypess AM, Chen YC, Sze C, et al. Cold but not sympathomimetics activates human brown adipose tissue in vivo. Proc Natl Acad Sci U S A 2012;109:10001–10005
4. Virtanen KA, Lidell ME, Orava J, et al. Functional brown adipose tissue in healthy adults. N Engl J Med 2009;360:1518–1525
5. Bartelt A, Bruns OT, Reimer R, et al. Brown adipose tissue activity controls triglyceride clearance. Nat Med 2011;17:200–205
6. Svensson KJ, Long JZ, Jedrychowski MP, et al. A secreted Slit2 fragment regulates adipose tissue thermogenesis and metabolic function. Cell Metab 2016;23:454–466
7. Stanford KI, Middelbeek RJW, Townsend KL, et al. Brown adipose tissue regulates glucose homeostasis and insulin sensitivity. J Clin Invest 2013;123:215–223
8. Wang GX, Zhao XY, Meng ZX, et al. The brown fat-enriched secreted factor Nrg4 preserves metabolic homeostasis through attenuation of hepatic lipogenesis. Nat Med 2014;20:1436–1443
9. Villarroya F, Cereijo R, Villarroya J, Giralt M. Brown adipose tissue as a secretory organ. Nat Rev Endocrinol 2017;13:26–35
10. Lynes MD, Leiria LO, Lundh M, et al. The cold-induced lipokine 12,13-diHOME promotes fatty acid transport into brown adipose tissue. Nat Med 2017;23:631–637
11. Thomou T, Mori MA, Dreyfuss JM, et al. Adipose-derived circulating miRNAs regulate gene expression in other tissues. Nature 2017;542:450–455
12. Arch JR. Challenges in β(3)-adrenoceptor agonist drug development. Ther Adv Endocrinol Metab 2011;2:59–64
13. Cawthorne MA, Sennitt MV, Arch JR, Smith SA. BRL 35135, a potent and selective atypical beta-adrenoceptor agonist. Am J Clin Nutr 1992;55:252S–257S
14. Weyer C, Tataranni PA, Snitker S, Danforth E Jr., Ravussin E. Increase in insulin action and fat oxidation after treatment with CL 316,243, a highly selective beta3-adrenoceptor agonist in humans. Diabetes 1998;47:1555–1561
15. Cypess AM, Weiner LS, Roberts-Toler C, et al. Activation of human brown adipose tissue by a β3-adrenergic receptor agonist. Cell Metab 2015;21:33–38
16. Protocol details. The mechanism of human non-shivering thermogenesis and basal metabolic rate [Internet]. Available from https://clinicalstudies.info.nih.gov/ProtocolDetails.aspx?A_2013-DK-0200.html. Accessed 7 June 2018
17. Malik M, van Gelderen EM, Lee JH, et al. Proarrhythmic safety of repeat doses of mirabegron in healthy subjects: a randomized, double-blind, placebo-, and active-controlled thorough QT study. Clin Pharmacol Ther 2012;92:696–706
18. Cypess AM, Lehman S, Williams G, et al. Identification and importance of brown adipose tissue in adult humans. N Engl J Med 2009;360:1509–1517
19. Chen KY, Brychta RJ, Linderman JD, et al. Brown fat activation mediates cold-induced thermogenesis in adult humans in response to a mild decrease in ambient temperature. J Clin Endocrinol Metab 2013;98:E1218–E1223
20. Leitner BP, Huang S, Brychta RJ, et al. Mapping of human brown adipose tissue in lean and obese young men. Proc Natl Acad Sci U S A 2017;114:8649–8654
21. Goldgof M, Xiao C, Chanturiya T, Jou W, Gavrilova O, Reitman ML. The chemical uncoupler 2,4-dinitrophenol (DNP) protects against diet-induced obesity and improves energy homeostasis in mice at thermoneutrality. J Biol Chem 2014;289:19341–19350
22. Tolstikov V, Nikolayev A, Dong S, Zhao G, Kuo MS. Metabolomics analysis of metabolic effects of nicotinamide phosphoribosyltransferase (NAMPT) inhibition on human cancer cells. PLoS One 2014;9:e114019
23. Drolet J, Tolstikov V, Williams BA, et al. Integrated metabolomics assessment of human dried blood spots and urine strips. Metabolites 2017;7:35
24. Gacias M, Gaspari S, Santos PM, et al. Microbiota-driven transcriptional changes in prefrontal cortex override genetic differences in social behavior. eLife 2016;5:e13442
25. Xia J, Wishart DS. Using metaboAnalyst 3.0 for comprehensive metabolomics data analysis. Curr Protoc Bioinformatics 2016;55:14.10.11–14.10.91
26. Chapple CR, Dvorak V, Radziszewski P, et al. A phase II dose-ranging study of mirabegron in patients with overactive bladder. Int Urogynecol J 2013;24:1447–1458
27. Enerbäck S, Jacobsson A, Simpson EM, et al. Mice lacking mitochondrial uncoupling protein are cold-sensitive but not obese. Nature 1997;387:90–94
28. Propping S, Newe M, Lorenz K, Wirth MP, Ravens U. β-Adrenoceptor-mediated relaxation of carbachol-pre-contracted mouse detrusor. Urol Int 2015;95:92–98
29. Lidell ME, Betz MJ, Dahlqvist Leinhard O, et al. Evidence for two types of brown adipose tissue in humans. Nat Med 2013;19:631–634
30. Dmitrieva NO, Almeida DM, Dmitrieva J, Loken E, Pieper CF. A day-centered approach to modeling cortisol: diurnal cortisol profiles and their associations among U.S. adults. Psychoneuroendocrinology 2013;38:2354–2365
31. Liu Z, Guo W. Modeling diurnal hormone profiles by hierarchical state space models. Stat Med 2015;34:3223–3234
32. Park HK, Ahima RS. Physiology of leptin: energy homeostasis, neuroendocrine function and metabolism. Metabolism 2015;64:24–34
33. Barrera JG, Sandoval DA, D'Alessio DA, Seeley RJ. GLP-1 and energy balance: an integrated model of short-term and long-term control. Nat Rev Endocrinol 2011;7:507–516
34. Yu H, Xia F, Lam KS, et al. Circadian rhythm of circulating fibroblast growth factor 21 is related to diurnal changes in fatty acids in humans. Clin Chem 2011;57:691–700
35. Brabant G, Ranft U, Ocran K, Hesch RD, von zur Mühlen A. Pulsatile pattern of thyrotropin-release in normal men. Clin Chim Acta 1986;155:159–162
36. Gavrilova O, Marcus-Samuels B, Reitman ML. Lack of responses to a beta3-adrenergic agonist in lipoatrophic A-ZIP/F-1 mice. Diabetes 2000;49:1910–1916
37. Gobel FL, Norstrom LA, Nelson RR, Jorgensen CR, Wang Y. The rate-pressure product as an index of myocardial oxygen consumption during exercise in patients with angina pectoris. Circulation 1978;57:549–556
38. Kitamura K, Jorgensen CR, Gobel FL, Taylor HL, Wang Y. Hemodynamic correlates of myocardial oxygen consumption during upright exercise. J Appl Physiol 1972;32:516–522
39. Larsen TM, Toubro S, van Baak MA, et al. Effect of a 28-d treatment with L-796568, a novel beta(3)-adrenergic receptor agonist, on energy expenditure and body composition in obese men. Am J Clin Nutr 2002;76:780–788
40. Redman LM, de Jonge L, Fang X, et al. Lack of an effect of a novel beta3-adrenoceptor agonist, TAK-677, on energy metabolism in obese individuals: a double-blind, placebo-controlled randomized study. J Clin Endocrinol Metab 2007;92:527–531
41. Sacco E, Bientinesi R. Mirabegron: a review of recent data and its prospects in the management of overactive bladder. Ther Adv Urol 2012;4:315–324
42. Chapple CR, Kaplan SA, Mitcheson D, et al. Mirabegron 50 mg once-daily for the treatment of symptoms of overactive bladder: an overview of efficacy and tolerability over 12 weeks and 1 year. Int J Urol 2014;21:960–967
43. Whittle AJ, Carobbio S, Martins L, et al. BMP8B increases brown adipose tissue thermogenesis through both central and peripheral actions. Cell 2012;149:871–885
44. Cypess AM, White AP, Vernochet C, et al. Anatomical localization, gene expression profiling and functional characterization of adult human neck brown fat. Nat Med 2013;19:635–639
45. Porter C, Herndon DN, Chondronikola M, et al. Human and mouse brown adipose tissue mitochondria have comparable UCP1 function. Cell Metab 2016;24:246–255
46. Oriowo MA, Thulesius O. Functional characterization of beta-adrenoceptors mediating relaxation in sheep gallbladder. Fundam Clin Pharmacol 1999;13:187–192
47. Trebicka J, Hennenberg M, Schulze Pröbsting A, et al. Role of beta3-adrenoceptors for intrahepatic resistance and portal hypertension in liver cirrhosis. Hepatology 2009;50:1924–1935

48. Samuel P, Saypoi GM, Meilman E, Mosbach EH, Chafizadeh M. Absorption of bile acids from the large bowel in man. J Clin Invest 1968;47:2070–2078
49. Dawson PA, Lan T, Rao A. Bile acid transporters. J Lipid Res 2009;50:2340–2357
50. Worthmann A, John C, Rühlemann MC, et al. Cold-induced conversion of cholesterol to bile acids in mice shapes the gut microbiome and promotes adaptive thermogenesis. Nat Med 2017;23:839–849
51. Repa JJ, Turley SD, Lobaccaro JA, et al. Regulation of absorption and ABC1-mediated efflux of cholesterol by RXR heterodimers. Science 2000;289:1524–1529
52. Goodwin B, Jones SA, Price RR, et al. A regulatory cascade of the nuclear receptors FXR, SHP-1, and LRH-1 represses bile acid biosynthesis. Mol Cell 2000;6:517–526
53. Chen Q, Amaral J, Oh S, Biancani P, Behar J. Gallbladder relaxation in patients with pigment and cholesterol stones. Gastroenterology 1997;113:930–937
54. Broeders EP, Nascimento EB, Havekes B, et al. The bile acid chenodeoxycholic acid increases human Brown adipose tissue activity. Cell Metab 2015;22:418–426
55. Deng Y, Wang ZV, Gordillo R, et al. An adipo-biliary-uridine axis that regulates energy homeostasis. Science 2017;355:eaaf5375
56. Jiang C, Xie C, Li F, et al. Intestinal farnesoid X receptor signaling promotes nonalcoholic fatty liver disease. J Clin Invest 2015;125:386–402
57. Berbée JF, Boon MR, Khedoe PP, et al. Brown fat activation reduces hypercholesterolaemia and protects from atherosclerosis development. Nat Commun 2015;6:6356
58. Wang GX, Zhao XY, Meng ZX, et al. The brown fat-enriched secreted factor Nrg4 preserves metabolic homeostasis through attenuation of hepatic lipogenesis. Nat Med 2014;20:1436–1443
59. Porez G, Prawitt J, Gross B, Staels B. Bile acid receptors as targets for the treatment of dyslipidemia and cardiovascular disease. J Lipid Res 2012;53:1723–1737
60. DuBois D, DuBois EF. A formula to estimate the approximate surface area if height and weight be known. Arch Intern Medicine. 1916;17:863–871